

Structures of the Ordered Water Monolayer on MgO(001)

Radosław Włodarczyk, Marek Sierka,* Karolina Kwapien, and Joachim Sauer

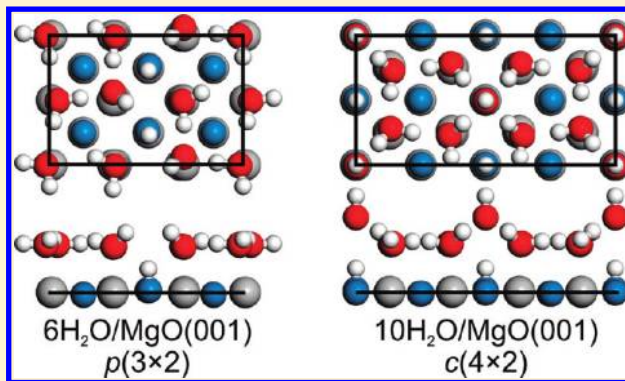
Institut für Chemie, Humboldt-Universität zu Berlin, Unter den Linden 6, 10099 Berlin, Germany

Esther Carrasco, Andreas Aumer, Janaina F. Gomes, Martin Sterrer,* and Hans-Joachim Freund

Department of Chemical Physics, Fritz-Haber-Institut der Max-Planck-Gesellschaft, Faradayweg 4-6, 14195 Berlin, Germany

Supporting Information

ABSTRACT: Global ab initio structure optimizations combined with statistical thermodynamics and experimental studies reveal atomic structures of the ordered water monolayer on the MgO(001) surface. Calculations based on density functional theory predict the existence of two stable surface structures: a $c(4 \times 2)$ structure containing ten water molecules per unit cell stable at low temperature and a $p(3 \times 2)$ structure containing six water molecules per unit cell stable at high temperature. Both structures feature four surface hydroxyl groups resulting from the dissociation of two water molecules per surface cell. The calculated properties of the two structures are in agreement with a multitude of experimental data, including infrared reflection absorption, sum frequency generation and X-ray photoelectron spectroscopy. Comparison of calculated and experimental vibrational spectra allows for assignment of the observed vibrational modes.



1. INTRODUCTION

The reactivity of water toward metal oxide surfaces is of fundamental interest in several fields such as biology, materials science, environmental science, geochemistry, and heterogeneous catalysis. Water adsorption on oxides is also central in understanding corrosion, passivation, and adhesion. It is therefore not surprising that the study of the structure of water at the interface with other materials continues to be a subject of particular interest in science, as demonstrated by the number of experimental^{1–3} and theoretical^{4–10} studies and several review papers.^{11–18} The MgO(001) surface is among the oxide surfaces that have received significant experimental^{1,19–29} and theoretical^{4,5,26,30–40} attention as a substrate for water adsorption. Structural and electronic simplicity of the MgO(001) surface as well as the fact that the dissociation of water on MgO plays an important role in many chemical processes are the main reasons for such extensive studies.⁴¹

The water monolayer on MgO(001) has received particular attention because it is one of the very few examples of water/oxide interfaces that give rise to an ordered adsorbed water layer. The first studies of water adsorption on ultrathin MgO(001)/Mo(001) films by Wu et al.⁴² using electron energy-loss spectroscopy (HREELS) and temperature programmed desorption (TPD) claimed heterolytic dissociation of H₂O on the surface. Later, Xu et al.⁴³ studied D₂O adsorbed on MgO(001)/Mo(001) thin films using TPD, reflection absorption infrared spectroscopy (IRAS), and low energy electron diffraction (LEED) and concluded

that (i) the water layer is adsorbed with the plane of D₂O molecules nominally parallel to the surface, (ii) D₂O does not undergo dissociation, and (iii) the unit cell contains a glide plane. In addition, a real space structure was proposed for D₂O adsorption on the MgO(001) surface with $p(3 \times 2)$ translational symmetry and an absolute coverage of 0.67 D₂O molecules per Mg cation. Heidberg et al.¹ investigated water adsorption on a cleaved MgO(001) single crystal using transmission Fourier transform infrared (FTIR) spectroscopy as well as LEED. They concluded that at 150 K H₂O forms an ordered monolayer with a $c(4 \times 2)$ translational symmetry and the molecular H₂O plane nearly parallel to the surface. LEED and helium atom scattering (HAS) experiments performed for water adsorbed under ultra-high vacuum conditions on MgO(001) single crystals suggested the presence of phases with $c(4 \times 2)$ and $p(3 \times 2)$ symmetry, with the transition from the $c(4 \times 2)$ to the less dense $p(3 \times 2)$ phase occurring at around 185 K.^{23–25} This transition is accompanied by a partial desorption of water, while the remaining monolayer phase is stable under UHV conditions up to 235 K.^{25,44} Additionally, it was confirmed that the unit cell of the high-temperature $p(3 \times 2)$ phase contains a glide plane.²³ The monolayer water coverage of the $p(3 \times 2)$ phase was estimated to be 1 ± 0.1 and the maximum water coverage prior to the onset of ice

Received: January 5, 2011

Revised: February 25, 2011

Published: March 17, 2011

formation to 1.3 ± 0.1 water molecules per MgO surface unit.^{25,44} Recently, experimental evidence for the presence of dissociated water in the monolayer was provided using metastable impact electron spectroscopy applied to water adsorbed at 90 K on the surface of well-ordered MgO(001) thin films.⁴⁵

The water adsorption on the MgO(001) surface was also extensively investigated using computational tools.^{4,5,8,34,35} Most of the studies^{4,34,35} focused on the $p(3 \times 2)$ phase of the H₂O/MgO(001) system with six adsorbed H₂O molecules per unit cell, as suggested by the experimental data.^{25,44} Using density functional theory (DFT), Giordano et al.⁴ obtained a structure in which glide plane symmetry was present. In this model the water monolayer is adsorbed almost flat with two out of six water molecules per unit cell dissociated. Two protons are donated to surface oxygen atoms and two hydrogen bonds are formed between water molecules twisted toward surface oxygen atoms. Starting from this model Delle Site et al.³⁴ found a more stable “flat dissociated structure” that maintains the glide plane. In this model two protons are donated to surface oxygen atoms; however, none of the water molecules is twisted and more hydrogen bonds are formed within the monolayer. Finally, Lynden-Bell et al.³⁵ performed an extended search for the structure that satisfies the observed $p(3 \times 2)$ symmetry constraints. Ten symmetry inequivalent structures were constructed with two dissociated and four nondissociated water molecules placed over the (3×2) MgO(001) surface unit cell. They found a new structure, which was slightly more stable than the “flat dissociated structure” and differed from it only by the relative orientations of H₂O molecules.

In contrast to the $p(3 \times 2)$ water adsorption structure theoretical investigations of the low-temperature $c(4 \times 2)$ water phase are scarce.^{33,36,39} Cho et al.³³ arranged four water molecules in the primitive $c(4 \times 2)$ cell and thus obtained the structure with monolayer water coverage of 1.0 water molecule per Mg atom. Jug et al.³⁹ performed cyclic cluster calculations for water coverage 1.0 and for a system consisting of 12 water molecules per (4×2) cell arranged in two 6-molecule layers. Finally, Jug et al.³⁶ carried out a molecular dynamics study of this two-layer adsorbate. However, so far no systematic search for the most stable model of the $c(4 \times 2)$ adsorption structure has been reported.

In this work we present results of a combined computational and experimental characterization of the ordered monolayer phases of water on MgO(001). Global ab initio structure optimizations on DFT potential energy surface combined with statistical thermodynamics reveal the most stable atomic structures. Monolayer related vibrational frequencies detected by infrared reflection absorption spectroscopy (IRAS) and sum frequency generation (SFG) spectroscopy are correlated to molecular and dissociated water signals obtained from X-ray photoelectron spectroscopy (XPS). The vibrational fingerprints are compared with the anharmonic frequencies calculated by molecular dynamics of the most stable $c(4 \times 2)$ and $p(3 \times 2)$ structure models, allowing a definite assignment of the observed vibrations to specific surface groups in the ordered phases.

2. COMPUTATIONAL DETAILS

2.1. Methods. All DFT calculations are performed using the Vienna Ab initio Simulation Package (VASP)^{46,47} along with the Perdew, Burke, and Ernzerhof (PBE)^{48,49} exchange–correlation functional. The electron-ion interactions are described by the projector augmented wave method (PAW), originally developed

by Blöchl⁵⁰ and adapted by Kresse and Joubert.⁵¹ Only the valence electrons are explicitly considered. A semiempirical c_6 -term is added to include the dispersion forces (PBE+D).^{52,53} Global structure optimizations using a genetic algorithm (GA)⁵⁴ are performed with a $2 \times 1 \times 1$ Monkhorst–Pack⁵⁵ k -point mesh and an energy cutoff of 250 eV. For the final structure optimizations and energy evaluations of the atomic structure models resulting from the GA calculations an energy cutoff of 400 eV and a $4 \times 2 \times 1$ k -point grid is applied. We note that the energies obtained with the first, lower accuracy setup generally reproduce, with a deviation of less than 0.05 eV, the ordering of the structures obtained at the second, higher level. All structure optimizations are carried out with a conjugate-gradient algorithm until the forces acting on ions are smaller than 10^{-3} eV/Å.

Calculations of the vibrational spectra within the harmonic approximation use a central finite difference method with 0.02 Å displacements of the atoms in each Cartesian direction. Intensities are obtained from the derivatives of the dipole moment component perpendicular to the surface. To compensate for systematic errors of DFT, the harmonic vibrational frequencies of H₂O/MgO(001) structures are scaled by an empirical factor of 0.9817 derived from a comparison between experimental⁵⁶ and calculated frequencies for the water molecule. To check the influence of anharmonic effects on the IR spectrum, we simulate the anharmonic infrared absorption spectra. To use a larger time step during the simulation, all hydrogen atoms are substituted by heavier deuterium atoms. Computations were carried out using molecular dynamics within the canonical (constant $T = 160$ K) ensemble with the algorithm of Nosé.⁵⁷ Calculations for 100 000 steps with time step of 0.25 fs are performed with a $2 \times 1 \times 1$ k -point mesh and a lower energy cutoff of 250 eV. The IR spectrum was obtained as the Fourier transform of the autocorrelation function of the classical dipole moment. To correct the intensities for the violation of the detailed balance conditions in the classical treatment and to account for hydrogen atom zero-point motion effects, we employ the quantum correction factor $\hbar\omega\beta/(1 - \exp(-\hbar\omega\beta))$.^{58,59} To compensate for the effect of the lower cutoff, the individual anharmonic bands are shifted by the differences of the corresponding harmonic vibrations calculated using 400 and 250 eV cutoffs.

2.2. Substrate Models. The equilibrium volume of the MgO unit cell is obtained assuming quadratic dependence of the energy on the cell volume and using a series of structures relaxed under fixed-volume condition. These calculations apply a $15 \times 15 \times 15$ Monkhorst–Pack k -point mesh and a plane-wave basis set with an energy cutoff of 1000 eV. This procedure yields a lattice constant of $a = 4.187$ Å ($Fm\bar{3}m$ symmetry), which is in good agreement with the experimentally determined lattice constant of 4.184 Å, corrected for the zero-point anharmonic expansion effect.⁶⁰ The slab structures are modeled using orthorhombic (3×2) and (4×2) MgO(001) supercells with lattice constants $a_0 = 8.883$, $b_0 = 5.922$ Å and $a_0 = 11.844$, $b_0 = 5.922$ Å, respectively. The surface is built of four MgO layers of which the two topmost are fully relaxed. The lattice parameter c_0 was set to 20 Å, which results in a vacuum layer of approximately 14 Å thickness (9.5 Å with maximum loading of water molecules), which is large enough to avoid surface–surface interactions.

2.3. Genetic Algorithm. Our implementation⁵⁴ of the genetic algorithm^{61,62} is a generalization of the algorithm introduced by Chuang et al.,⁶² in which different surface structures form a population. The algorithm starts with a population of 50–60

Table 1. Water Coverages ($n\text{H}_2\text{O}$ Molecules per (1×1) $\text{MgO}(001)$ Surface) of the Studied Systems

unit cell	$n \text{H}_2\text{O}/\text{unit cell}$	coverage
3×2	5	0.83
4×2	7	0.88
3×2	6	1.00
4×2	8	1.00
4×2	9	1.13
3×2	7	1.17
4×2	10	1.25
3×2	8	1.33

adsorption structures obtained by a random distribution of a stoichiometric number of H and O atoms on a given $\text{MgO}(001)$ surface model (Table 1). The structures in the initial pool are optimized to the nearest local minimum. The evolution from one generation to the next one takes place by crossover. For this two structures are selected from the population to be parents for crossover. The selection process uses a roulette wheel selection⁶¹ with the selection probability being proportional to the value of the fitness function of a given structure. The fitness is obtained as a function of the dynamically scaled relative energy ε_i ,

$$\varepsilon_i = \frac{E_i - E_{\min}}{E_{\max} - E_{\min}} \quad (1)$$

where E_i is the total energy of the given member of the population, and E_{\min} and E_{\max} correspond to the lowest and highest total energies in the population. The normalized fitness f_i is then assessed on an exponential scale

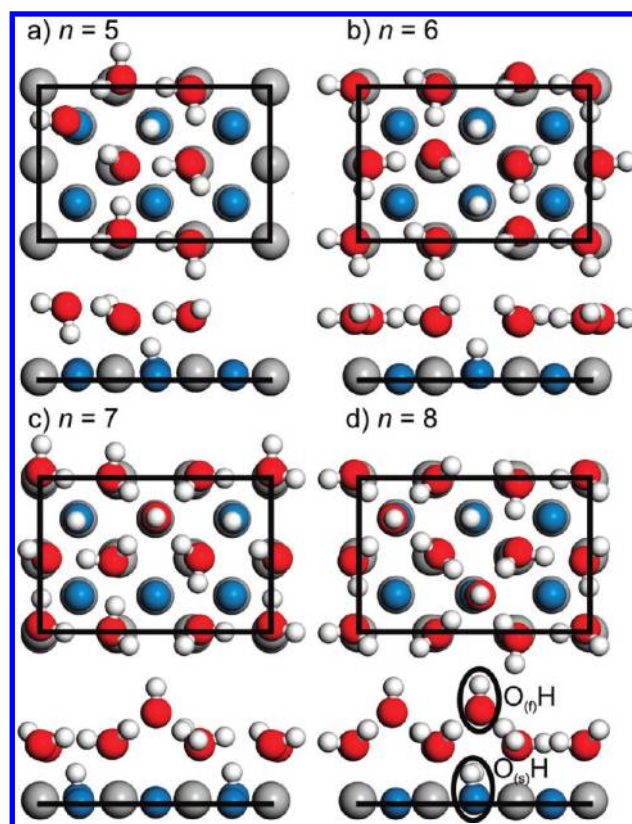
$$f_i = \frac{\exp(-\alpha\varepsilon_i)}{\sum_j \exp(-\alpha\varepsilon_j)} \quad (2)$$

where α is a constant. This definition of f_i automatically increases the selection pressure with a decreasing range of energies E_i in the population.^{63,64} The crossover operation adapted in our implementation is similar to the one used by Chuang et al.,⁶² in which parent structures are sectioned by an arbitrary plane and recombined to create a child structure. The child structure is accepted if all of the following conditions are fulfilled: (i) there are no pairs of atoms with unreasonably small interatomic distances; (ii) there are no unbound atoms; (iii) the chemical composition is maintained; (iv) the new structure is significantly different than all structures obtained so far during the GA run. The 10–15 child structures are optimized to the nearest local minimum. A new population, consisting of 20–30 structures, is formed from the parent structures of the current generation and the most stable optimized children structures.

3. EXPERIMENTAL DETAILS

The experiments were performed in two separate UHV facilities. One is equipped with LEED, infrared spectroscopy (Bruker IFS 66v), X-ray photoelectron spectroscopy (XPS, Specs), and TPD as analytical tools. The other one was used to record sum frequency generation (SFG) spectra.

$\text{Ag}(001)$ single crystals were used as substrate for thin MgO films. The $\text{Ag}(001)$ surface was cleaned by repeated sputter (Ar^+) – anneal (700 K) cycles. Thin $\text{MgO}(001)$ films of typically 13 monolayer thickness were grown by reactive deposition of Mg in

**Figure 1.** Side and top views of the most stable $n\text{H}_2\text{O}/(3 \times 2)$ structure models (Mg gray, O red and blue, H white).

oxygen (1×10^{-6} mbar) at a substrate temperature of 600 K and at a rate of 1 monolayer/min. Crystallinity and cleanliness of $\text{Ag}(001)$ and $\text{MgO}(001)$ were checked with LEED and XPS. D_2O (99.9% Aldrich) was adsorbed on the MgO thin films via background dosing using a leak valve. Prior to admission to the chamber, D_2O was degassed by repeated freeze–pump–thaw cycles. Exposures are given in langmuir units ($1 \text{ langmuir} = 1.33 \times 10^{-6} \text{ mbar} \cdot \text{s}$). The temperature of the crystal was $\sim 85 \text{ K}$ during adsorption.

XPS data were acquired using an $\text{Al K}\alpha$ X-ray source ($h\nu = 1486.6 \text{ eV}$, 100 W) with a Phoibos150 analyzer equipped with a multichannel detector. A takeoff angle of 60° was used to increase surface sensitivity. It has been reported that synchrotron-based and conventional X-ray sources might cause photoinduced water dissociation.^{65,66} This possibility can be disregarded in the present study since two successive XPS spectra acquired at the same spot on a water dosed sample are equivalent to each other. However, an initial small desorption of water from the sample during XP spectra acquisition, which is equivalent to a temperature increase of about 5 K, could be observed by checking the IRAS spectra before and after XPS measurements. The deconvolution of the XPS spectra was performed by fitting Gaussian-broadened Lorentzian shapes after Shirley background correction. The shapes and fwhm have been fixed and propagated along the series of spectra.

IRAS spectra were obtained by accumulating 1000 scans with a resolution of 4 cm^{-1} . The spectrum of a clean $\text{MgO}(001)$ film was used as background. The heating rate in TPD experiments was 1 K/s.

SFG vibrational spectroscopy was performed using a Nd:YAG laser (1064 nm, 30 mJ/pulse, 25 ps, 50 Hz) with part of the

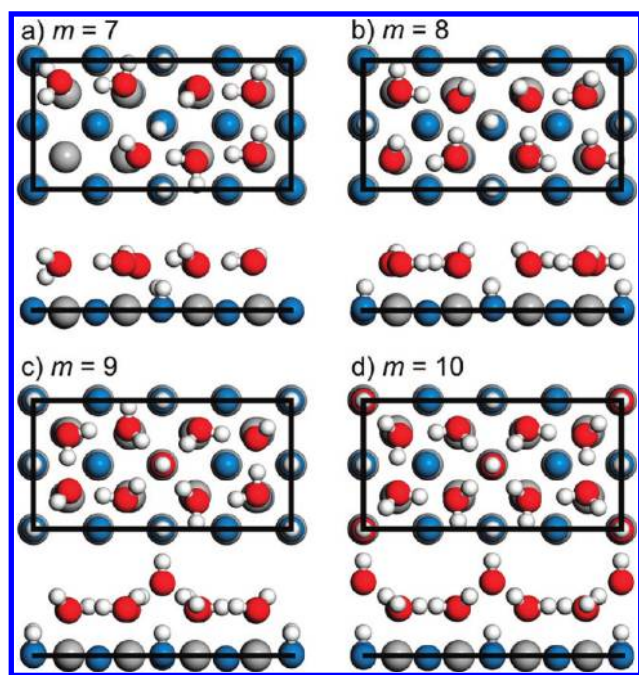


Figure 2. Side and top views of the most stable $m\text{H}_2\text{O}/(4\times 2)$ structure models (Mg gray, O red and blue, H white).

output converted to 532 and 355 nm by a harmonic generator. The 1064 and 355 nm beams were mixed in an optical parametric generator/difference frequency generator to produce tunable infrared pulses of about 50–150 $\mu\text{J}/\text{pulse}$ in the range 2.5–6 μm , with a resolution of about 5 cm^{-1} . The 532 nm light used for SFG had an energy of about 200 $\mu\text{J}/\text{pulse}$. The measured SFG intensities were normalized by the intensity of the incident IR beam.

4. COMPUTATIONAL RESULTS

4.1. Structures. Figures 1 and 2 show the most stable structures of $n\text{H}_2\text{O}/(3\times 2)$, $n = 5-8$, and $m\text{H}_2\text{O}/(4\times 2)$, $m = 7-10$, water surface layers found by GA simulations. In all structures water undergoes partial dissociation with proton transfer to the MgO surface oxygen atoms. These “surface” OH groups are denoted as $\text{O}_{(s)}\text{H}$. The hydroxyl groups which remain within the H_2O monolayer after H_2O dissociation are denoted as $\text{O}_{(f)}\text{H}$ groups (cf. Figure 1d). Generally, dispersion correction improves the accuracy of DFT calculations with the PBE exchange–correlation functional.⁵² However, in the present case no significant influence on the atomic structures has been found. Below we discuss specific features of individual global minimum structures.

$5\text{H}_2\text{O}/(3\times 2)$: This structure (Figure 1a) contains one dissociated water molecule per unit cell. The water monolayer is arranged in stripes separated by voids of about 3 Å in width. The molecular plane of one H_2O molecule is twisted perpendicularly to the surface with a distance between the hydrogen and surface O atoms of only 1.56 Å. All other water molecules are arranged with their molecular plane almost parallel to the surface.

$6\text{H}_2\text{O}/(3\times 2)$: Global optimization of this system yields the known structure³⁵ with a pg plane symmetry plane, as shown in Figure 1b. The water monolayer is virtually flat (molecular planes of H_2O parallel to the surface) and two water molecules are dissociated. All O atoms of the water molecules are placed

directly above surface Mg sites. The $\text{O}_{(s)}\text{H}$ groups are arranged along one of the glide planes.

$7\text{H}_2\text{O}/(3\times 2)$: This structure also contains two dissociated water molecules per unit cell (Figure 1c). A particular feature of this structure is that the $\text{O}_{(f)}\text{H}$ group oriented perpendicularly to the surface plane is coordinated by hydrogen atoms of four nearby water molecules. This motif is present in all structure models with water coverages higher than one molecule per Mg atom.

$8\text{H}_2\text{O}/(3\times 2)$. This is the system with the highest water coverage examined in this work (cf. Table 1). Two water molecules per unit cell are dissociated and the water monolayer contains two $\text{O}_{(f)}\text{H}$ groups oriented perpendicularly to the surface plane and coordinated by hydrogen atoms of four nearby water molecules (Figure 1d).

$7\text{H}_2\text{O}/(4\times 2)$: In this structure two water molecules per unit cell are dissociated, as shown in Figure 2a. Similarly to the global minimum of $5\text{H}_2\text{O}/(3\times 2)$, the water monolayer is not completely flat, and one H_2O molecule is twisted with the hydrogen atom pointing toward the surface O atom and a H–O distance of 1.69 Å.

$8\text{H}_2\text{O}/(4\times 2)$. Three water molecules per unit cell are dissociated with molecular planes of H_2O oriented parallel to the surface (Figure 2b). The $\text{O}_{(f)}\text{H}$ groups are tilted up out of the surface. This structure differs significantly from those investigated by Cho et al.³³ and Jug et al.³⁹ Their structure models show $c(4\times 2)$ unit cells, different from the $p(4\times 2)$ unit cell of the present model. Furthermore, both authors considered only even numbers of dissociated water molecules (0, 2, and 4) per unit cell (three is the most stable in our model). In fact, the structure suggested by Cho et al. is less stable by 0.41 eV/(unit cell) than the present model.

$9\text{H}_2\text{O}/(4\times 2)$: The global minimum structure contains three dissociated H_2O molecules per unit cell. The surface layer belongs to the $p2$ surface symmetry group, as shown in Figure 2c. One $\text{O}_{(f)}\text{H}$ group is oriented perpendicularly to the surface plane and is coordinated by hydrogen atoms of four nearby water molecules.

$10\text{H}_2\text{O}/(4\times 2)$: The global minimum structure (Figure 2d) belongs to the cm surface symmetry group and contains a mirror plane and a glide plane. Two water molecules per unit cell are dissociated with both $\text{O}_{(f)}\text{H}$ groups oriented perpendicularly to the surface plane and coordinated by hydrogen atoms of four surrounding water molecules.

Jug et al.³⁹ also investigated $12\text{H}_2\text{O}/(4\times 2)$ structures with 2, 4, and 6 dissociated water molecules. This water coverage of 1.5 molecules per Mg surface atom is higher than suggested by TPD experiments.^{25,44} Their structures consist of two layers of H_2O , each containing six molecules, and leave one of the surface Mg atoms not coordinated by H_2O . In our models Mg atoms not coordinated by H_2O or OH^- are found only in structures with water coverage smaller than 1.0, namely for $5\text{H}_2\text{O}/(3\times 2)$ and $7\text{H}_2\text{O}/(4\times 2)$. Additionally, in their model with six dissociated water molecules per unit cell one of the Mg atoms moved out of the surface. According to our calculations all structures with Mg atoms located above the surface plane of MgO(001) are considerably less stable than structures with intact surface.

We note that water clusters larger than a hexamer tend to form 3-D networks of intact, H-bonded molecules,⁶⁷ whereas the structures shown here form 2-D networks incorporating dissociated molecules. This clearly shows the significant influence of the MgO substrate.

4.2. Stability Analysis. The stability of the different $n\text{H}_2\text{O}/\text{MgO}(001)$ surface models is compared using the Gibbs free energy, ΔG , for adsorption of n water molecules on a clean MgO(001)

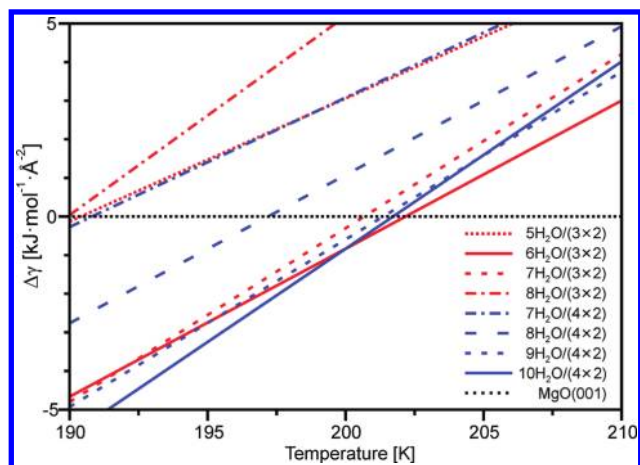


Figure 3. Surface Gibbs free energy of formation $\Delta\gamma(T, p = 10^{-10}$ mbar) of the $n\text{H}_2\text{O}/(3\times 2)$ and $m\text{H}_2\text{O}/(4\times 2)$ models as a function of temperature.

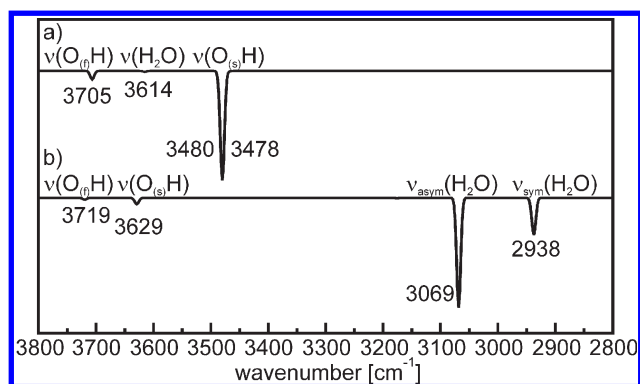
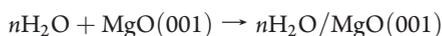


Figure 4. Simulated harmonic IR spectra for (a) $6\text{H}_2\text{O}/(3\times 2)$ and (b) $10\text{H}_2\text{O}/(4\times 2)$. Frequencies are scaled by a factor of 0.9817.

surface



per surface area A , defined as

$$\Delta\gamma = \frac{\Delta G}{A}$$

Figure 3 displays $\Delta\gamma$ at a pressure of $p = 10^{-10}$ mbar as a function of temperature T for the most stable $n\text{H}_2\text{O}/\text{MgO}(001)$ structure models found. It demonstrates the existence of only two stable phases for water adsorption on the $\text{MgO}(001)$ surface: $10\text{H}_2\text{O}/(4\times 2)$ and $6\text{H}_2\text{O}/(3\times 2)$ surface layers. The $10\text{H}_2\text{O}/(4\times 2)$ structure is stable up to $T = 200$ K and the $6\text{H}_2\text{O}/(3\times 2)$ structure between 200 and 202 K. Increasing the temperature above 202 K results in complete desorption of water from the $\text{MgO}(001)$ surface.

4.3. Vibrational Spectra. In this section we discuss only vibrations that are active in the frequency region investigated by the present experiments, i.e., above 2800 and 2000 cm^{-1} for H_2O and D_2O structures, respectively. Figure 4 shows the harmonic vibrational spectra computed for the most stable $6\text{H}_2\text{O}/(3\times 2)$ and $10\text{H}_2\text{O}/(4\times 2)$ structure models. The IR spectrum of the $6\text{H}_2\text{O}/(3\times 2)$ model (Figure 4a) contains only four active vibrations at 3705 , 3614 , 3480 , and 3478 cm^{-1} . The

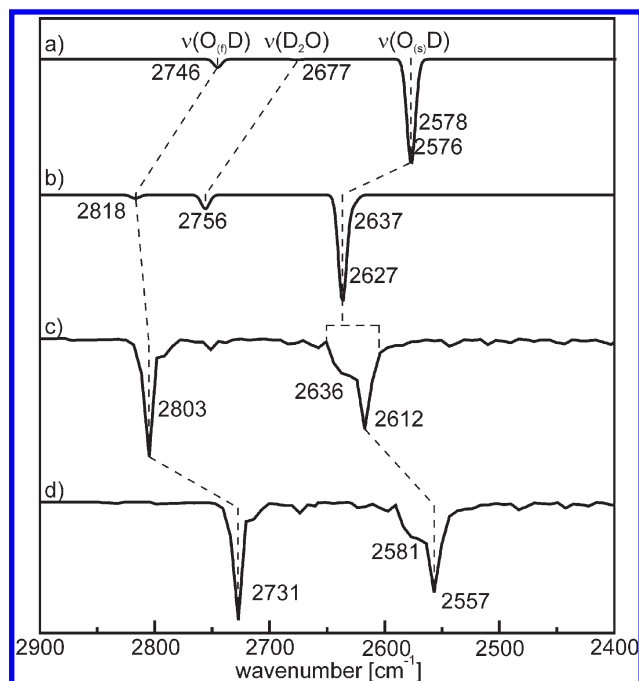


Figure 5. Simulated IR spectra for the most stable $6\text{D}_2\text{O}/(3\times 2)$ structure model: (a) harmonic (400 eV cutoff); (b) harmonic (250 eV cutoff); (c) anharmonic (250 eV cutoff); (d) anharmonic spectrum corrected for the effect of a lower cutoff (see text for details).

two former vibrations at 3705 and 3614 cm^{-1} correspond to the $\nu(\text{O}_{(f)}-\text{H})$ and $\nu(\text{O}-\text{H})$ stretching modes of the $\text{O}_{(f)}\text{H}$ groups and H_2O molecules, respectively (see Figure S.1, Supporting Information). The two vibrations at 3480 and 3478 cm^{-1} correspond to the $\nu(\text{O}_{(s)}-\text{H})$ stretching modes of the surface $\text{O}_{(s)}\text{H}$ hydroxyl groups and are considerably red-shifted with respect to the $\nu(\text{O}_{(f)}-\text{H})$ vibrations due to hydrogen bonding with neighboring water molecules. The harmonic spectrum computed for the $10\text{H}_2\text{O}/(4\times 2)$ model (Figure 4b) shows two weak features at 3719 and 3629 cm^{-1} , which are assigned to the $\nu(\text{O}_{(f)}-\text{H})$ and $\nu(\text{O}_{(s)}-\text{H})$ stretching modes, respectively, and two very intense bands at 3069 and 2938 cm^{-1} . The two intense vibrations can be described as combinations of the asymmetric and symmetric O–H stretching vibrations of water molecules coordinating the $\text{O}_{(f)}\text{H}$ group (see Figure S.2, Supporting Information). These vibrations are characteristic for $\text{O}_{(f)}\text{H}$ groups oriented perpendicularly to the surface plane and coordinated by hydrogen atoms of four nearby water molecules. Such groups are present in all models with water coverage higher than one molecule per magnesium atom.

To facilitate comparison with experimental spectra, we have also calculated anharmonic IR spectra of the two most stable $6\text{D}_2\text{O}/(3\times 2)$ and $10\text{D}_2\text{O}/(4\times 2)$ structure models. Figure 5 shows a comparison of the computed harmonic and anharmonic IR spectra obtained for the $6\text{D}_2\text{O}/(3\times 2)$ structure. The harmonic spectrum shows the same features as the corresponding spectrum of the $6\text{H}_2\text{O}/(3\times 2)$ structure in Figure 4a. The use of a lower cutoff for the plane wave basis set introduces blue shifts of 72 and 55 cm^{-1} for the $\nu(\text{O}_{(f)}-\text{D})$ and $\nu(\text{O}_{(s)}-\text{D})$ harmonic vibrational bands, respectively (Figure 5a,b). These values are used to correct the anharmonic spectrum as shown in Figure 5c,d. For the assignment of vibrational bands in the anharmonic spectrum and to facilitate comparison with the experimental

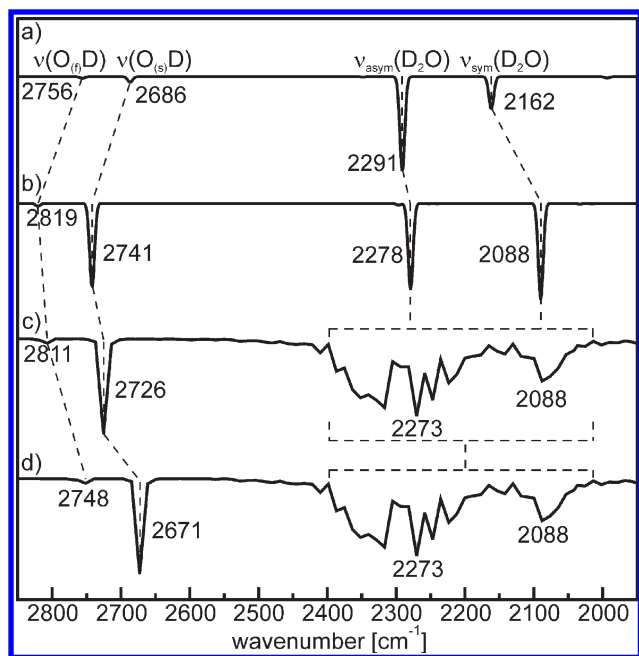


Figure 6. Simulated IR spectra for the most stable $10\text{D}_2\text{O}/(4\times 2)$ structure model: (a) harmonic (400 eV cutoff); (b) harmonic (250 eV cutoff); (c) anharmonic (250 eV cutoff); (d) anharmonic spectrum corrected for the effect of a lower cutoff (see text for details).

spectra reported below, we performed Fourier transforms of the z -velocity autocorrelation function for the individual deuterium atoms (Figure S.3, Supporting Information). This approach is consistent with the surface selection rule, which applies to the thin film samples used in this study and according to which only vibrational modes with a component of the dynamic dipole moment perpendicular to the surface will contribute to the experimental spectrum (e.g., ref 68). The analysis shows that the band at 2731 cm^{-1} in the corrected anharmonic spectrum corresponds to the $\nu(\text{O}(\text{f})-\text{D})$ stretching mode, whereas the broad bands at 2581 and 2557 cm^{-1} are assigned to different combinations of the $\nu(\text{O}(\text{s})-\text{D})$ stretching vibrations. The remaining water molecules in this structure do not contribute to the IR spectrum due to their almost flat adsorption geometry. Figure 6 shows the comparison of computed harmonic and anharmonic IR spectra for the $10\text{D}_2\text{O}/(4\times 2)$ structure model. The harmonic spectrum shows the same features as the corresponding spectrum of the $10\text{H}_2\text{O}/(4\times 2)$ structure (Figure 4b). The use of a lower cutoff for the plane wave basis set increases the intensity of the $\nu(\text{O}(\text{s})-\text{D})$ stretching mode and introduces blue shifts of 63 and 55 cm^{-1} to the $\nu(\text{O}(\text{f})-\text{D})$ and $\nu(\text{O}(\text{s})-\text{D})$ harmonic vibrations, respectively (Figure 6a,b). These values are used to correct the anharmonic spectrum as shown in Figure 6c,d. We do not apply such a correction to the broad band at $2020\text{--}2400\text{ cm}^{-1}$. The corrected anharmonic spectrum shows a sharp band at 2671 cm^{-1} and a broad signal between 2020 and 2400 cm^{-1} . The Fourier transforms of the z -velocity autocorrelation function of the individual deuterium atoms reveal that the 2671 cm^{-1} signal corresponds to the $\nu(\text{O}(\text{s})-\text{D})$ stretching mode and the broad $2020\text{--}2400\text{ cm}^{-1}$ band corresponds to a combination of stretching modes of D_2O molecules (Figure S.4, Supporting Information). The intensity of the $\nu(\text{O}(\text{f})-\text{D})$ mode is negligible compared to the remaining vibrations.

5. EXPERIMENTAL RESULTS

5.1. Temperature-Programmed Desorption. Figure 7a shows TPD spectra obtained for water adsorbed at 90 K on the surface of a 20 monolayer $\text{MgO}(001)/\text{Ag}(001)$ film. In agreement with earlier studies a high temperature desorption peak at 215 K related to desorption from the D_2O monolayer on $\text{MgO}(001)$ is observed for low water coverage. With increasing coverage an additional desorption peak at 150 K , showing zeroth-order desorption, grows in, which is due to sublimation of ice multilayers. In general, the TPD spectra agree well with the results of similar measurements on $\text{MgO}(001)$ single crystals and $\text{MgO}(001)/\text{Mo}(001)$ thin films reported previously.^{43,44} Two details are worth noting: (i) there is no significant desorption of water at temperatures above the monolayer desorption peak, which is indicative for an only small abundance of defects giving rise to water dissociation on the $\text{MgO}(001)$ surface. (ii) In the region $160\text{--}190\text{ K}$, between multilayer and monolayer desorption, a desorption plateau is observed, indicating some desorption of water molecules. In this temperature range a small desorption peak has been attributed to the transition of the water monolayer from the $c(4\times 2)$ to the $p(3\times 2)$ phase.²³

5.2. X-ray Photoelectron Spectroscopy. The series of photoemission spectra collected at different sample temperatures presented in Figure 7b resembles the changes of water coverage during desorption detected by TPD. After initial adsorption of 5 langmuirs of D_2O at 90 K , an intense peak due to the three-dimensional amorphous ice layer is observed in the $\text{O}1\text{s}$ region at 534.8 eV . In addition, a contribution of the oxide O^{2-} peak, which is strongly attenuated due to the presence of a thick ice layer, is seen at 530.1 eV . The chemical shift of 4.7 eV is consistent with molecular water in the three-dimensional ice network.¹³ Increasing the temperature to 150 K leads to partial desorption of the ice multilayer. Concomitantly, the oxide peak increases in intensity whereas the molecular water peak decreases. At 152 K , the multilayer water is completely desorbed accompanied by a substantial decrease in intensity of the molecular water peak together with a shift of 0.8 eV (to 534.0 eV) to lower binding energy. A similar BE shift, in reverse order, has been observed on various surfaces as the first water layer is filled and subsequent multilayers start to grow and has been generally ascribed to final-state screening effects.¹³ Upon further annealing to 180 K , the intensity of the peak at higher binding energy decreases, indicating partial desorption of water from the surface. A further decrease of its peak intensity takes place after heating to 190 K until at 200 K and above water is almost completely desorbed. Note that 200 K is already at the leading edge of the water desorption peak observed by TPD. Since XPS and also IRAS spectra reported below were acquired after the base pressure in the chamber has returned to a value of below 10^{-9} mbar after each temperature increase, complete desorption of the monolayer is accomplished already at 200 K .

The spectrum obtained at a temperature of 170 K is presented in Figure 7c together with the deconvolution into its components. A perfect fitting of the spectrum requires, apart from the molecular water and the oxide peaks at 534.0 and 530.1 eV , respectively, a third component at intermediate binding energy, 532.5 eV . This component can be assigned to surface hydroxyls (deuterohydroxyls) according to its chemical shift of 2.4 eV to higher binding energy with respect to the oxide peak.²⁰ This observation is consistent with a previous experimental finding, where the presence of hydroxyls in the water monolayer on well ordered

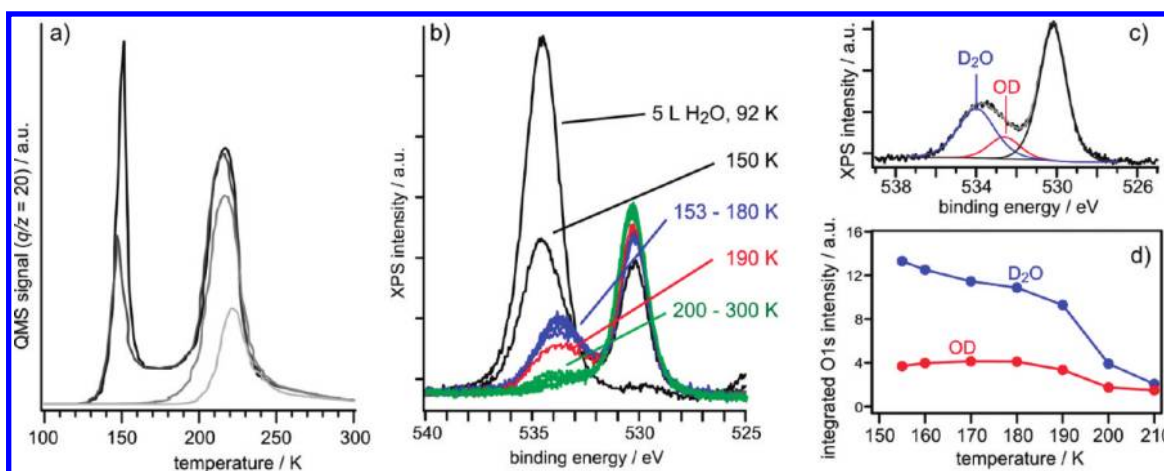


Figure 7. (a) TPD spectra of increasing doses (0.3–2 langmuirs) of D_2O adsorbed at 90 K on $MgO(001)/Ag(001)$. (b) XPS spectra of the O1s region after adsorption of 5 langmuirs of D_2O and subsequent annealing to the indicated temperatures. (c) XPS spectrum obtained after 170 K annealing together with the different components used in the fit. (d) Temperature dependence of the integrated O1s intensities according to molecular water and hydroxyl species in the water monolayer obtained from fits of the XPS spectra presented in (b).

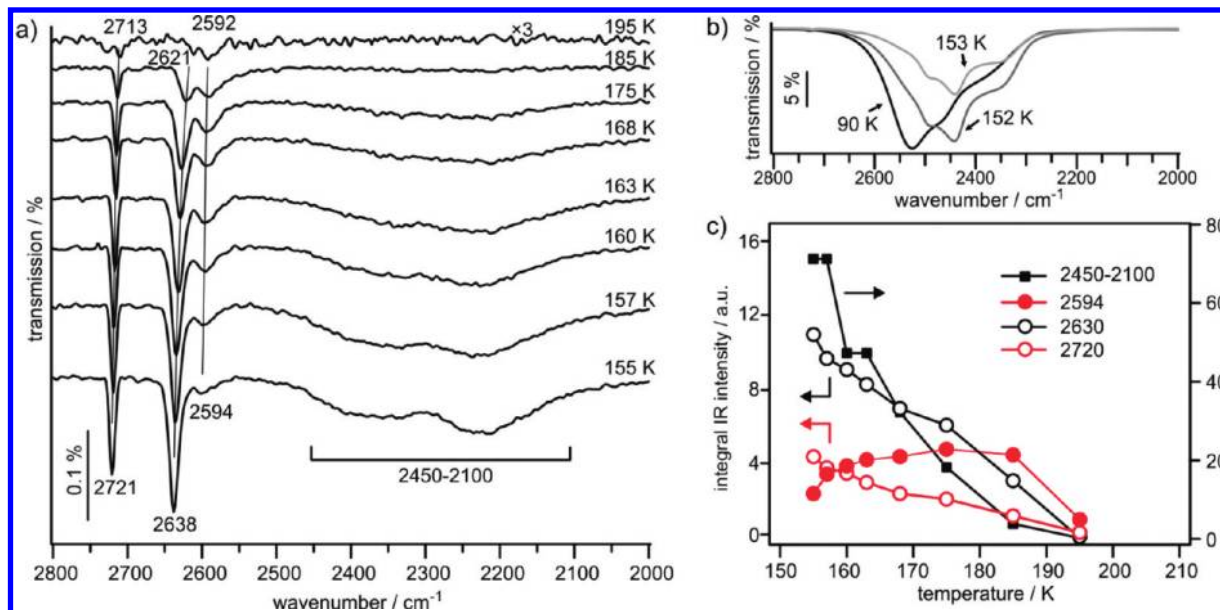


Figure 8. (a) Series of IRAS spectra after initial adsorption of 20 langmuirs of D_2O on $MgO(001)/Ag(001)$ and annealing to the indicated temperatures. (b) IRAS spectra of ice multilayers. (c) Temperature dependence of the integral intensities of OD signal components obtained from fits of the IRAS spectra presented in (a).

$MgO(001)/Mo(001)$ thin films after water adsorption at 90 K has been detected with MIES.⁴⁵ The representation of the absolute intensities of the water-related O1s emission peaks with respect to the annealing temperature in Figure 7d shows that a continuous desorption of molecular water takes place in the temperature range where the monolayer is stable. A correlation between this behavior and the desorption plateau between multi- and monolayer desorption observed in the TPD spectra (Figure 7a) is obvious. In contrast, the concentration of surface hydroxyls slightly increases in the temperature range 155 to 180 K, and is then, with the onset of monolayer desorption above 190 K, reduced to a constant background value. The disappearance of the hydroxyl species at this temperature provides evidence that they are related to the water monolayer and not to water dissociated at surface defects. The presence of both

molecularly and dissociatively adsorbed water in the water monolayer regime on $MgO(001)$ is in agreement with previous DFT calculations.^{4,34}

5.3. Infrared Reflection Absorption Spectroscopy. IRAS spectra recorded in UHV in the temperature range 90–200 K after initial adsorption of 20 langmuirs of D_2O at 90 K are presented in Figure 8. Figure 8b shows the spectra obtained in the multilayer water regime. At 90 K, water forms an amorphous water regime. The band maximum shifts from 2530 to 2440 cm^{-1} by increasing the temperature to 152 K, characteristic for the transition from amorphous to crystalline ice (Figure 8b). Further increase of temperature leads to multilayer desorption until at 155 K the IR spectrum simplifies considerably and is composed of three sharp bands at 2721, 2638, and 2594 cm^{-1} , as well as two

broad features centered at 2380 and 2220 cm^{-1} , respectively (Figure 8a). (The three sharp bands are correspondingly shifted to 3688, 3576, and 3508 cm^{-1} , when H_2O is used instead of D_2O .) With increasing temperature, the sharp monolayer signals slightly shift to lower wavenumber. Notably, the spectral intensity of both the bands initially present at 2721 and 2638 cm^{-1} progressively decreases, whereas the one of the lower frequency signal at 2594 cm^{-1} appears to stay almost constant. Only after heating at 195 K have all sharp monolayer IRAS signals significantly lost intensity, and no signals are observed at temperatures higher than 195 K. The broad signals at 2380 and 2220 cm^{-1} decrease also in intensity until 170 K and are completely absent at temperatures of 185 K and above. Spectral fitting of the monolayer IRAS signals yields the temperature dependence of the respective integral intensities displayed in Figure 8c. The result confirms the progressive intensity decrease of the signals at 2720 and 2636 cm^{-1} , as well as of the broad bands between 2500 and 2100 cm^{-1} . On the other hand, the intensity of the signal at 2594 cm^{-1} initially increases up to 175 K, stays almost constant thereafter, and decreases only after heating to 195 K.

The observed frequencies in the water monolayer regime correspond well with results of previous studies: For water adsorbed on the surface of $\text{MgO}(001)/\text{Mo}(001)$ thin films, Xu et al.⁴³ observed signals at 2714, 2637, and 2571 cm^{-1} by IRAS. Using polarized infrared spectroscopy in transmission, Heidberg et al.¹ studied water adsorption on UHV-cleaved $\text{MgO}(001)$ single crystals and found the respective vibrations at 2710, 2676, and 2597 cm^{-1} , as well as broad features in the range 2600–2200 cm^{-1} . The assignment of the observed vibrational features has been discussed controversially. While Heidberg et al. attributed the broad absorption between 2600 and 2200 cm^{-1} to the strong hydrogen bonding network present in the $c(4\times 2)$ monolayer phase, and the sharp signals to the symmetric and asymmetric stretch vibrations of monomeric water as well as to dangling OH of water bound to steps, Xu et al. assigned the broad features to multilayer ice and the sharp ones to tilted water molecules adsorbed on unoccupied Mg sites in the $p(3\times 2)$ phase or at domain walls. In neither of these studies have hydroxyl groups being considered as giving rise to certain vibrations, because theoretical and experimental evidence for their presence was obtained only later.

The XPS results presented in Figure 7b,c provide evidence that the amount of hydroxyl groups slightly increases in the temperature range 155–180 K. The only infrared signal that does not decrease in intensity in this temperature range is the absorption at 2594 cm^{-1} , which suggests that this band can be assigned to hydroxyl groups resulting from dissociated water molecules in the monolayer. In addition, the continuous intensity decrease of the broad IR bands at 2450–2100 cm^{-1} , which are undoubtedly related to molecular D_2O in a strong hydrogen bonding network, relates to the loss of molecular water between 155 and 190 K observed with XPS. The interpretation of the signals at 2720 and 2630 cm^{-1} is less obvious. IR signals above 2720 cm^{-1} are in general assigned to dangling (or free) OD groups, whereas the signal at 2630 cm^{-1} falls into the range where both D–O–D stretching vibrations of water molecules and the stretching vibration of surface deuteroxyl groups are expected. The continuous intensity decrease of the signal at 2630 cm^{-1} between 155 and 190 K would be in line with the XPS result of desorbing molecular water in this range. It could, however, also be related to the loss of deuteroxyl groups of the $c(4\times 2)$ monolayer phase during its transformation into the $p(3\times 2)$ phase, which occurs in this temperature range. To obtain

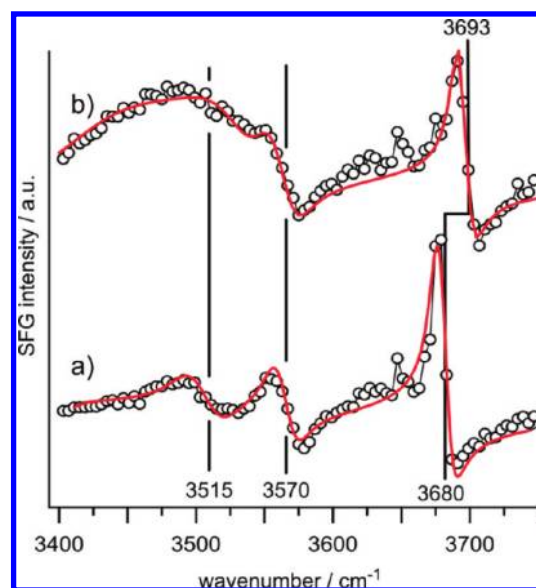


Figure 9. (a) SFG spectrum of H_2O monolayer on $\text{MgO}(001)/\text{Ag}(001)$ obtained after adsorption of 20 langmuirs of H_2O at 90 K and subsequent heating to 160 K. (b) SFG spectrum after adsorption of additional 20 langmuirs of H_2O at 90 K.

more information about the properties of the sharp vibrational signals observed in the OD stretching region, SFG experiments were conducted.

5.4. Sum Frequency Generation Spectroscopy. In the special case considered here SFG spectroscopy offers, due to its interface sensitivity, the possibility to investigate the interactions of molecular species of the water monolayer on $\text{MgO}(001)$ with multilayer water molecules. This is due to the fact that in SFG the signal contribution from multilayer water is by far smaller than in comparable infrared spectroscopic experiments, which allows us, therefore, to track the changes of monolayer vibrational features upon adsorption of additional ice layers. In Figure 9a the SFG spectrum of monolayer water on $\text{MgO}(001)$ thin films, which has been obtained after adsorption of 20 langmuirs of H_2O at 90 K and subsequent heating to 160 K, is shown. In accordance with the IRAS data presented in Figure 8a, three signals are observed, which, because H_2O was used instead of D_2O , are found at 3680, 3570, and 3515 cm^{-1} . Upon adsorption of additional 20 langmuirs of H_2O at 90 K, some broad resonances due to the thick ice layer appear at the low frequency side of the spectrum. The monolayer signal at 3570 cm^{-1} does not change in intensity and frequency after additional adsorption of H_2O (Figure 9b). The second monolayer signal at 3515 cm^{-1} is partly obscured by the ice resonances and, therefore, difficult to discern in the SFG spectrum in Figure 9b. However, spectral fitting reveals that also this component remains almost unchanged. This result suggests that these two monolayer species are not affected by adsorption of water and, therefore, do not significantly interact with second layer H_2O molecules. In contrast, the signal at 3680 cm^{-1} is replaced by a higher frequency signal at 3693 cm^{-1} . The latter can be assigned to free OH groups on the surface of the ice multilayer. The disappearance of the 3680 cm^{-1} absorption results from hydrogen bonding interaction of the corresponding monolayer species with second layer water molecules, which shifts its frequency to lower values.

The SFG results prove that the high frequency signal at 2720 (3680) cm^{-1} can be assigned to free OH groups, which, because they stick out of the monolayer, are prone to interact with second layer water molecules. On the other hand, the molecular species giving rise to the signals at 2630 and 2594 cm^{-1} do not interact with second layer water molecules. Therefore, they are constituents of the water monolayer that are screened from the surrounding.

6. DISCUSSION

Ordered structures of the water monolayer on MgO(001) have been the subject of various experimental and computational studies in the past. While diffraction studies provided evidence for the presence of both $c(4\times 2)$ and $p(3\times 2)$ type H_2O overlayers,^{1,23–25,43} the interpretation of the vibrational features observed with infrared spectroscopy has so far been inconclusive. The present study provides an assignment of the observed vibrational signals to specific structural elements in the stable H_2O monolayer phases.

The global ab initio optimization procedure combined with thermodynamic analysis provides evidence for the existence of two stable monolayer structures, one with $c(4\times 2)$ symmetry and 10 water molecules per unit cell, and one with $p(3\times 2)$ symmetry and 6 water molecules per unit cell. The experimentally determined monolayer water coverage for the $p(3\times 2)$ ($\Theta = 1 \pm 0.1$) and $c(4\times 2)$ phases ($\Theta = 1.3 \pm 0.1$)^{25,44} is in excellent agreement with calculated values for $6\text{H}_2\text{O}/(3\times 2)$ and $10\text{H}_2\text{O}/(4\times 2)$ structure models ($\Theta = 1.0$ and 1.25, respectively). The most stable $6\text{H}_2\text{O}/(3\times 2)$ structure with 2 dissociated water molecules per unit cell found in this study is in agreement with results of previous computational studies.³⁵ In addition, we provide a new structural model for the $c(4\times 2)$ phase, also containing two dissociated water molecules per unit cell. The most stable low-temperature phase is the $10\text{H}_2\text{O}/(4\times 2)$ structure, which, upon temperature increase, transforms into the $6\text{H}_2\text{O}/(3\times 2)$ that is then stable until complete monolayer desorption. According to our calculations all water adsorption phases become less stable than the clean MgO(001) surface for temperatures higher than 202 K, which explains the single desorption peak observed at 215 K in the TPD experiment (Figure 7a). The small difference between calculated and experimental desorption peak temperature can easily be caused by the limited accuracy of the DFT method. The small desorption peak at 185 K observed in previous TPD studies is in line with the transition from the $10\text{H}_2\text{O}/(4\times 2)$ to the less dense $6\text{H}_2\text{O}/(3\times 2)$ monolayer phase, which is accompanied by desorption of a fraction of the monolayer water molecules. The fact that instead of a clear peak a desorption plateau in the range 160–190 K is observed between monolayer and multilayer desorption in the present study (Figure 7a) is most probably related to the smaller MgO island size on MgO(001)/Ag(001) thin films as compared to vacuum-cleaved MgO(001) single crystals.

The use of a thin MgO film significantly simplifies the vibrational response of the ordered water monolayer, because only vibrations with a dipole moment perpendicular to the surface are registered due to the metal surface selection rule. The analysis of the simulated spectra reveals contributions of basically three types of structural elements found in both stable monolayer phases: $\text{O}_{(\text{f})}\text{D}$, $\text{O}_{(\text{s})}\text{D}$, and molecular D_2O . The free OD groups, $\text{O}_{(\text{f})}\text{D}$, resulting from D_2O dissociation, exhibit the highest frequencies, which are similar in both the $10\text{D}_2\text{O}/(4\times 2)$

and $6\text{D}_2\text{O}/(3\times 2)$ monolayer phase. The surface OD groups, $\text{O}_{(\text{s})}\text{D}$, are found at lower frequency than the $\text{O}_{(\text{f})}\text{D}$ groups, with the one from the $6\text{D}_2\text{O}/(3\times 2)$ structure shifted more strongly than $\text{O}_{(\text{s})}\text{D}$ in $10\text{D}_2\text{O}/(4\times 2)$ due to different hydrogen bonding environments. In the $6\text{D}_2\text{O}/(3\times 2)$ phase molecular water is oriented almost parallel to the surface; thus it is not expected to contribute to the IRAS spectrum of a thin film sample. Its calculated stretching frequency, 2677 cm^{-1} , is in the range of frequencies that are typical for low density water layers on solid surfaces. In contrast, water molecules stabilizing the protruding $\text{O}_{(\text{f})}\text{D}$ group in the $10\text{D}_2\text{O}/(4\times 2)$ structure are slightly tilted and lead to strong vibrational contributions in the range 2400–2020 cm^{-1} . With the help of the simulated vibrational spectra we can now identify specific vibrational features observed in experiment. At low temperature, after desorption of the multilayer, the vibrational spectrum is characterized by a broad absorption in the range 2450–2100 cm^{-1} , as well as of two sharp absorptions at 2721 and 2638 cm^{-1} (Figure 8a). The SFG spectrum reported in Figure 9 provided evidence that the signal at 2721 cm^{-1} can be assigned to a $\text{O}_{(\text{f})}\text{D}$ group, whereas the sharp signal at 2638 cm^{-1} is screened from the surrounding and does not interact with second layer water molecules. The observed features are very similar to the simulated spectrum of the $10\text{D}_2\text{O}/(4\times 2)$ structure (Figure 6), which identifies the signals at 2721 and 2638 cm^{-1} as $\text{O}_{(\text{f})}\text{D}$ and $\text{O}_{(\text{s})}\text{D}$ groups, respectively, in line with the SFG result, and the broad contributions in the range 2450–2100 cm^{-1} to water molecules coordinating the $\text{O}_{(\text{f})}\text{D}$ group. On the other hand, at the highest temperature where vibrational features can still be observed, the spectrum contains a sharp signal at 2713 cm^{-1} and a broader one at 2592 cm^{-1} , in agreement with the vibrational signature of the $6\text{D}_2\text{O}/(3\times 2)$ structure obtained in the simulation (Figure 5), with the 2713 cm^{-1} signal identified as the $\text{O}_{(\text{f})}\text{D}$ group and the 2592 cm^{-1} signal as $\text{O}_{(\text{s})}\text{D}$. The progressive decrease of signal intensity of both the broad bands at low frequency and the sharp signal at 2638 cm^{-1} , as well as the initial increase of the 2592 cm^{-1} feature, reflect the gradual transformation of the (4×2) into the (3×2) structure with increasing temperature (Figure 8a). This is reflected also in the slightly increasing OH coverage in the temperature range 155–180 K as obtained from XPS. The IRAS data indicate that, in the present study, both water monolayer phases are simultaneously present on the surface of the MgO thin films, with the $c(4\times 2)$ structure more abundant at low temperature, and the $p(3\times 2)$ structure dominating just before monolayer desorption.

The thermodynamic analysis presented in Figure 3 is in perfect agreement with previous HAS studies reporting on the stability range of the $c(4\times 2)$ and $p(3\times 2)$ water monolayer structures on MgO(001). With the new models and vibrational analysis we may now also reinterpret previous infrared spectroscopic data obtained for the water monolayer. In the polarized IR spectra published by Heidberg et al.¹ all vibrational features predicted for the $10\text{D}_2\text{O}/(4\times 2)$ and $6\text{D}_2\text{O}/(3\times 2)$ structural models are present. At low temperature they observed a broad absorption in the range 2200–2600 cm^{-1} as well as two sharp ones at 2715 and ~ 2630 cm^{-1} (the latter signal has not been discussed in ref 1 but can clearly be seen in the spectra). With the help of LEED measurements carried out under the same experimental conditions, the low-temperature spectra have been attributed to a $c(4\times 2)$ overlayer. This interpretation together with the observed vibrational signals is in perfect agreement with the result of the present study for the $10\text{D}_2\text{O}/(4\times 2)$ structure.

Moreover, three sharp IR signals at 2710, 2676, and 2597 cm^{-1} have been observed at around 190 K, which were assigned to water molecules at steps and terraces on the MgO surface. With the vibrational analysis reported here, these spectrum contributions can be identified as arising from the $6\text{D}_2\text{O}/(3\times 2)$ structure. Similarly, the vibrational spectra reported by Xu et al.⁴³ obtained from water monolayers on MgO/Mo(001) thin films contain vibrational features that are in line with the interpretation of $10\text{D}_2\text{O}/(4\times 2)$ and $6\text{D}_2\text{O}/(3\times 2)$ structures found here.

In contrast to diffraction studies, which reveal the symmetry of the H_2O overlayer on MgO(001), the analysis of vibrational frequencies provides a more atomistic view of the monolayer structure. The excellent agreement of calculated and experimental vibrational spectra strongly suggests that the structural models proposed in the present study realistically represent the water monolayer structures present on the MgO(001) surface.

7. SUMMARY AND CONCLUSIONS

Atomic structures of the water monolayer adsorbed on the MgO(001) surface have been determined by global ab initio structure optimizations in combination with statistical thermodynamics and experimental studies. The calculated phase diagram reveals two stable surface structures. The low-temperature phase is composed of ten water molecules per unit cell with $c(4\times 2)$ symmetry. At higher temperature the structure containing six water molecules per unit cell with $p(3\times 2)$ symmetry is the most stable phase. In both structures adsorbed water undergoes partial dissociation forming surface hydroxyl groups, with two dissociated water molecules per unit cell. Both the unit cell symmetry and water coverage are in excellent agreement with experimental data. The calculated anharmonic spectra for the two stable monolayer structures are in excellent agreement with experimental vibrational spectra and allow for the assignment of the observed IR frequencies to specific structural elements of the water monolayer.

■ ASSOCIATED CONTENT

S Supporting Information. Simulated anharmonic spectra, selected normal vibrational modes, and side and top view of structure models. This material is available free of charge via the Internet at <http://pubs.acs.org>.

■ AUTHOR INFORMATION

Corresponding Author

*Electronic mail: M. Sierka, marek.sierka@chemie.hu-berlin.de; M. Sterrer, sterrer@fhi-berlin.mpg.de.

■ ACKNOWLEDGMENT

This work was supported by the Cluster of Excellence "Unifying Concepts in Catalysis" sponsored by the Deutsche Forschungsgemeinschaft DFG and administrated by the Technische Universität Berlin. E.C. thanks the Spanish Ministry of Science and Innovation for a fellowship. M.S. thanks Fabio Finocchi for fruitful discussions.

■ REFERENCES

(1) Heidberg, J.; Redlich, B.; Wetter, D. *Ber. Bunsenges. Phys. Chem.* **1995**, *99*, 1333.

- (2) Eng, P. J.; Trainor, T. P.; Brown, G. E., Jr.; Waychunas, G. A.; Newville, M.; Sutton, S. R.; Rivers, M. L. *Science* **2000**, *288*, 1029.
- (3) Ketteler, G.; Yamamoto, S.; Bluhm, H.; Andersson, K.; Starr, D. E.; Ogletree, D. F.; Ogasawara, H.; Nilsson, A.; Salmeron, M. *J. Phys. Chem. C* **2007**, *111*, 8278.
- (4) Giordano, L.; Goniakowski, J.; Suzanne, J. *Phys. Rev. Lett.* **1998**, *81*, 1271.
- (5) Odelius, M. *Phys. Rev. Lett.* **1999**, *82*, 3919.
- (6) Hass, K. C.; Schneider, W. F.; Curioni, A.; Andreoni, W. *Science* **1998**, *282*, 265.
- (7) Zhang, C.; Lindan, P. J. D. *J. Chem. Phys.* **2003**, *118*, 4620.
- (8) Costa, D.; Chizallet, C.; Ealet, B.; Goniakowski, J.; Finocchi, F. *J. Chem. Phys.* **2006**, *125*, 054702.
- (9) Vener, M. V.; Rozanska, X.; Sauer, J. *Phys. Chem. Chem. Phys.* **2009**, *11*, 1702–1712.
- (10) Hofmann, A.; Sauer, J. *J. Phys. Chem. B* **2004**, *108*, 14652.
- (11) Thiel, P. A.; Madey, T. E. *Surf. Sci. Rep.* **1987**, *7*, 211.
- (12) Brown, G. E.; Henrich, V. E.; Casey, W. H.; Clark, D. L.; Eggleston, C.; Felmy, A.; Goodman, D. W.; Gratzel, M.; Maciel, G.; McCarthy, M. I.; Neelson, K. H.; Sverjensky, D. A.; Toney, M. F.; Zachara, J. M. *Chem. Rev.* **1999**, *99*, 77.
- (13) Henderson, M. A. *Surf. Sci. Rep.* **2002**, *46*, 1.
- (14) Al-Abadleh, H. A.; Grassian, V. H. *Surf. Sci. Rep.* **2003**, *52*, 63.
- (15) Grassian, V. H. *Surf. Sci.* **2008**, *602*, 2955.
- (16) Verdager, A.; Sacha, G. M.; Bluhm, H.; Salmeron, M. *Chem. Rev.* **2006**, *106*, 1478.
- (17) Batzill, M.; Diebold, U. *Prog. Surf. Sci.* **2005**, *79*, 47.
- (18) Fenter, P.; Sturchio, N. C. *Prog. Surf. Sci.* **2004**, *77*, 171.
- (19) Foster, M.; Furse, M.; Passno, D. *Surf. Sci.* **2002**, *502–503*, 102.
- (20) Liu, P.; Kendelewicz, T.; Brown, G. E.; Parks, G. A. *Surf. Sci.* **1998**, *412–413*, 287.
- (21) Abriou, D.; Jupille, J. *Surf. Sci.* **1999**, *430*, L527.
- (22) Peng, X. D.; Barteau, M. A. *Surf. Sci.* **1990**, *233*, 283.
- (23) Ferry, D.; Glebov, A.; Senz, V.; Suzanne, J.; Toennies, J. P.; Weiss, H. *J. Chem. Phys.* **1996**, *105*, 1697.
- (24) Ferry, D.; Glebov, A.; Senz, V.; Suzanne, J.; Toennies, J. P.; Weiss, H. *Surf. Sci.* **1997**, *377–379*, 634.
- (25) Ferry, D.; Picaud, S.; Hoang, P. N. M.; Girardet, C.; Giordano, L.; Demirdjian, B.; Suzanne, J. *Surf. Sci.* **1998**, *409*, 101.
- (26) Kim, Y. D.; Lynden-Bell, R. M.; Alavi, A.; Stulz, J.; Goodman, D. W. *Chem. Phys. Lett.* **2002**, *352*, 318.
- (27) Finocchi, F.; Hacquart, R.; Naud, C.; Jupille, J. *J. Phys. Chem. C* **2008**, *112*, 13226.
- (28) Demirdjian, B.; Suzanne, J.; Ferry, D.; Coulomb, J. P.; Giordano, L. *Surf. Sci.* **2000**, *462*, L581.
- (29) Foster, M.; D'Agostino, M.; Passno, D. *Surf. Sci.* **2005**, *590*, 31.
- (30) Giordano, L.; Goniakowski, J.; Suzanne, J. *Phys. Rev. B* **2000**, *62*, 15406.
- (31) Finocchi, F.; Goniakowski, J. *Phys. Rev. B* **2001**, *64*, 125426.
- (32) Longo, E.; Varela, J. A.; Senapeschi, A. N.; Whitemore, O. J. *Langmuir* **1985**, *1*, 456.
- (33) Cho, J.-H.; Park, J. M.; Kim, K. S. *Phys. Rev. B* **2000**, *62*, 9981.
- (34) Delle Site, L.; Alavi, A.; Lynden-Bell, R. M. *J. Chem. Phys.* **2000**, *113*, 3344.
- (35) Lynden-Bell, R. M.; Delle Site, L.; Alavi, A. *Surf. Sci.* **2002**, *496*, L1.
- (36) Jug, K.; Heidberg, B.; Bredow, T. *J. Phys. Chem. C* **2007**, *111*, 6846.
- (37) Ferrari, A. M.; Roetti, C.; Pisani, C. *Phys. Chem. Chem. Phys.* **2007**, *9*, 2350.
- (38) Gay, I. D.; Harrison, N. M. *Surf. Sci.* **2005**, *591*, 13.
- (39) Jug, K.; Heidberg, B.; Bredow, T. *Surf. Sci.* **2007**, *601*, 1529.
- (40) Minot, Ch. *Surf. Sci.* **2004**, *562*, 237.
- (41) Henrich, V. E.; Cox, P. A. *The Surface Science of Metal Oxides*, Cambridge University Press: Cambridge, 1994.
- (42) Wu, M.-C.; Estrada, C. A.; Corneille, J. S.; Goodman, D. W. *J. Chem. Phys.* **1992**, *96*, 3892.
- (43) Xu, C.; Goodman, D. W. *Chem. Phys. Lett.* **1997**, *265*, 341.

- (44) Stirniman, M. J.; Huang, C.; Smith, R. S.; Joyce, S. A.; Kay, B. D. *J. Chem. Phys.* **1996**, *105*, 1295.
- (45) Kim, Y. D.; Stultz, J.; Goodman, D. W. *J. Phys. Chem. B* **2002**, *106*, 1515.
- (46) Kresse, G.; Furthmüller, J. *Comput. Mater. Sci.* **1996**, *6*, 15.
- (47) Kresse, G.; Furthmüller, J. *Phys. Rev. B* **1996**, *54*, 11169.
- (48) Perdew, J. P.; Burke, K.; Ernzerhof, M. *Phys. Rev. Lett.* **1996**, *77*, 3865.
- (49) Perdew, J. P.; Burke, K.; Ernzerhof, M. *Phys. Rev. Lett.* **1997**, *78*, 1396.
- (50) Blöchl, P. E. *Phys. Rev. B* **1994**, *50*, 17953.
- (51) Kresse, G.; Joubert, D. *Phys. Rev. B* **1999**, *59*, 1758.
- (52) Grimme, S. *J. Comput. Chem.* **2006**, *27*, 1787.
- (53) Kerber, T.; Sierka, M.; Sauer, J. *J. Comput. Chem.* **2008**, *29*, 2088.
- (54) Sierka, M. *Prog. Surf. Sci.* **2010**, *85*, 398.
- (55) Monkhorst, H. J.; Pack, J. D. *Phys. Rev. B* **1976**, *13*, 5188.
- (56) Shimanouchi, T. *Natl. Stand. Ref. Data Ser., Natl. Bur. Stand.*, **1972**, 39.
- (57) Nosé, S. *Mol. Phys.* **1984**, *52*, 255.
- (58) Gaigeot, M.-P.; Sprik, M. *J. Phys. Chem. B* **2003**, *107*, 10344.
- (59) Borysow, J.; Moraldi, M.; Frommhold, L. *Mol. Phys.* **1985**, *56*, 913.
- (60) Csonka, G. I.; Perdew, J. P.; Ruzsinszky, A.; Philipsen, P. H. T.; Lebegue, S.; Paier, J.; Vydrov, O. A.; Ángyán, J. G. *Phys. Rev. B* **2009**, *79*, 155107.
- (61) Goldberg, D. E. *Genetic Algorithms in Search, Optimization & Machine Learning*, Addison-Wesley: Boston, 2005.
- (62) Chuang, F. C.; Ciobanu, C. V.; Shenoy, V. B.; Wang, C. Z.; Ho, K. M. *Surf. Sci.* **2004**, *573*, L375.
- (63) Johnston, R. L. *Dalton Trans.* **2003**, 4193–4207.
- (64) Wales, D. J. *Energy Landscapes with Applications to Clusters, Biomolecules and Glasses*, Cambridge University Press: Cambridge, 2003.
- (65) Pirug, G.; Knauff, O.; Bonzel, H. P. *Surf. Sci.* **1994**, *321*, 58.
- (66) Tzvetkov, G.; Zubavichus, Y.; Koller, G.; Schmidt, T.; Heske, C.; Umbach, E.; Grunze, M.; Ramsey, M. G.; Netzer, F. P. *Surf. Sci.* **2003**, *543*, 131.
- (67) Lee, H. M.; Suh, S. B.; Lee, J. Y.; Tarakeshwar, P.; Kim, K. S. *J. Chem. Phys.* **2000**, *112*, 9759.
- (68) Hoffmann, F. M. *Surf. Sci. Rep.* **1983**, *3*, 107.